Citation: Olivar, M., T. Yokoi, T. Hayashida (2021), Site effects estimation from strong ground motion and microtremor records around the city of Tsukuba, Synopsis of IISEE-GRIPS Master's Thesis.

SITE EFFECTS ESTIMATION FROM STRONG GROUND MOTION AND MICROTREMOR RECORDS AROUND THE CITY OF TSUKUBA

Mónica Beatriz Olivar Amaya[1,2] **Supervisor: Toshiaki YOKOI[3], Takumi HAYASHIDA[3]**

ABSTRACT

We obtained the site effects from two strong motion observation sites around the City of Tsukuba, with strong ground motion and microtremor records. We estimated the Horizontal-to-Horizontal Spectral Ratio (HHSR), which is a direct estimation of the site amplification, and the Horizontal-to-Vertical Spectral Ratio (HVSR) from 13 earthquakes recorded at a KiK-NET station. We also calculated the HVSR for microtremor records from measurements of a broadband seismometer and a strong motion accelerometer, and the dispersion curves of Rayleigh waves from array measurements performed with broadband seismometers, and short period sensors. With these products we performed the joint inversion analysis and obtained the S-wave velocity structure for three groups of data: the reference group, when we perform a single point measurement and array measurements with broadband sensors; the group called Case-1, when we perform a single point measurement with a broadband sensor, but do not have enough broadband seismometers to perform an array, so we use short period seismometers; and the group called Case-2, when we do not have any broadband sensor to perform single point and array measurements. This way we highlighted the necessity of a broadband sensor to perform this type of analysis. Additionally, we estimated the theoretical site amplification factor, with the velocity structure obtained from the joint inversion of the reference data. We concluded that we can obtain a reliable inverted velocity structure with at least, one broadband sensor. The theoretical amplification factor based on the reference inverted velocity structure can give a good and reliable estimation of the amplification factor of the site. The HVSR of earthquakes and microtremor records cannot be regarded as site amplification factor, however, they are useful to determine the resonant frequencies.

Keywords: Site Effects, Joint Inversion, Broadband Sensor, Microtremor.

1. INTRODUCTION

This study is aimed to perform a case study of site effect estimate in a well-controlled condition with borehole records, and an application of the latest methods for microtremor records, including the application of the seismic interferometry. The target area is the central part of Tsukuba City, where the Building Research Institute (BRI) and the National Research Institute for Earth Science and Disaster Resilience (NIED) keep strong motion observation stations, among them Tsukuba City Hall (TKC) and IBRH10, respectively. Additionally, it is intended to emphasize the necessity of a broadband sensor to perform the analysis of the site characterization, estimating the S-wave velocity structure and the site

[1] GENSAI Project II, El Salvador.
[2] IISEE-GRIPS Master's course student.
[3] International Institute of Seismology and Earthquake Engineering, Building Research Institute.

amplification, and to check the feasibility of using the HVSR of Strong Motion records in place of the Broadband sensor. The results of this study will be very useful to apply the technology and methods for the seismic hazard assessment in the Metropolitan Area of San Salvador, El Salvador.

2. DATA

The target area of this study is the City of Tsukuba, located at the rim of the tectonic Kanto basin, about 60 km North-East of Tokyo. The strong-motion observation sites used in this study are located around the central part of Tsukuba City. The analyzed sites are IBRH10, a KiK-NET Strong Motion Observation Station deployed by the NIED; and TKC in Tsukuba City Office deployed by the BRI to observe seismic response of this base-isolated building of 7 stories, of which a sensor is installed at the basement floor. IBRH10 is located on fluvial sediment of the Holocene age, and TKC is located on middle terrace of Late Pleistocene epoch. In this study we selected thirteen earthquakes with magnitudes from 4 to 6, of which epicenters are near the target sites. We also use the information of the velocity structure measured at the borehole of IBRH10 for comparison.

For the microtremor analysis we use the records for IBRH10 and TKC stations shown in Table 1.

Table 1: Microtremor single point and array measurements

IBRH10 Measurements	TKC Measurements
3 channel single point measurement (CMG40T, [0.033-50] Hz)	
3 channel single point measurement (JEP6A3, Accelerometer 2[V/G])	
7 points array (VSE12-CC [0.05-100] Hz side lenght: 600 m, 40 m, radius: 2 m)	3 points triangular array (CMG40T, side length: 35 m)
7 points array (L22D, 2 Hz, radius: 2 m)	7 points array (L22D 2 Hz, side length: 4 m, 8 m)

3. METHODOLOGY

3.1. Direct Estimation of Site Amplification Factor and HVSR of Strong Motion and Microtremor Records

The soil-to-rock spectral ratio HHSR(EQ) for strong motion directly provides the amplification factor of the S wave and it can be determined utilizing the strong ground motion records obtained from the surface and from the borehole drilled into bedrock. On the other hand, the HVSR is used to assess the resonance frequencies of the surface soil layers. In this study, we apply the Fast Fourier Transform to obtain the Fourier Spectra and then, we estimate the HHSR(EQ), HVSR(EQ) and HVSR(MT) with the quadratic mean formula (Arai and Tokimatsu, 2004).

For the strong motion records, we calculate the HHSR for the S-wave windows, with widths of 10.24 seconds measured from the S-wave onset; we calculate the HVSR(EQ) for the S-coda windows with widths of 81.92 seconds taken from 20 seconds after the S-wave onset. For the microtremor records, to calculate the HVSR(MT) we use different time windows depending on the how often traffic noises appear in the records.

3.2. Spatial AutoCorrelation (SPAC) Method

The SPAC method was proposed by Aki (1957; 1965). This method allows to determine the phase velocity of surface waves that comes from different directions recorded by a bi-dimensional array of seismographs, where the vertical component of the microtremor records is dominated by Rayleigh waves. According to Okada (2003), the coherence function (SPAC coefficient) is obtained by the azimuthal average of coherency between microtremor records observed by two sensors, and it is written as:

$$\rho(r_{AB},\omega)=\frac{1}{2\pi}\int_0^{2\pi}\frac{E[\emptyset(\omega,r,\theta)]}{E[\emptyset(\omega,0,0)]}d\theta=\frac{1}{2\pi}\int_0^{2\pi}\frac{Re\{E[C_{A,B}(\omega,r)]\}}{E[C_{A,A}(\omega)]}d\theta=J_0\left(\frac{r\omega}{c(\omega)}\right)\ , \qquad (1)$$

where $\rho(r_{AB},\omega)$ is the SPAC coefficient; $A(0,0)$ and $B(r,0)$ represent the location of the sensors; $E[\,]$ is the ensemble average over time blocks; Re denotes the real part of a complex number; $C_{A,B}(\omega)$ is the cross-spectrum between sensors A and B; $C_{A,A}(\omega)$ is the power spectrum of sensor A; $J_0\left(\frac{r\omega}{c(\omega)}\right)$ is the zero order Bessel Function of the first kind; and $c(\omega)$ is the phase velocity.

3.3. Joint Inversion of HVSR(MT) and Dispersion Curves of Rayleigh Waves

In this study, we perform the joint inversion of the HVSR(MT) and the Dispersion Curves of Rayleigh waves using the diffuse field theory (HV-Inv, García-Jerez *et al*., 2016). This method shows the possibility of recovering the Green's functions under the diffuse wavefield conditions (Salinas *et al*., 2014), it is derived from the energy equipartition principle (Sánchez-Sesma *et al*., 2011). It has been established that if we assume that the seismic noise is diffuse, it is possible to express the HVSR(MT) in terms of the imaginary part of the Green's function. The imaginary part of the frequency domain Green's function for a receiver and source that are coincident at the location x, measures the injected power into the system by the unit harmonic load u_m, considering waves emitted and returned to the source; this allows us to express the directional energy density at a point x as:

$$E_m(x,\omega)=\rho\omega^2\langle u_m(x,\omega)u_m^*(x,\omega)\rangle=-2\pi\mu E_s k^{-1}\mathrm{Im}[G_{mm}(x,x,\omega)]\ , \qquad (2)$$

where ρ is the mass density; ω is the angular frequency; μ is the elastic shear modulus; k is the shear wave number; E_s is the average density of shear waves; and $\mathrm{Im}[G_{mm}(x,x,\omega)]$ is the imaginary part of the Green's function of the displacement x in the direction m, produced by a unit load coincident with the same direction and point.

HVSR(MT) can be expressed as:

$$[H/V](x,\omega)=\sqrt{\frac{E_1(x,\omega)+E_2(x,\omega)}{E_3(x,\omega)}}=\sqrt{\frac{\mathrm{Im}[G_{11}(x,x,\omega)]+\mathrm{Im}[G_{22}(x,x,\omega)]}{\mathrm{Im}[G_{33}(x,x,\omega)]}}\ , \qquad (3)$$

where $E_1, E_2,$ and E_3 are the directional energy density at a point x, allow us to obtain the theoretical HVSR(MT) for the specific geometry and material properties of a site: α_i, β_i, ρ_i, and h_i. The parameters correspond to the P-wave and S-wave velocities, mass density, and thickness of the i-th layer, respectively, of a ground structure made of isotropic elastic layers.

4. RESULTS AND DISCUSSION

The result of the HVSR and SPAC analysis are shown in Figure 1, where Figure 1a and Figure 1b show the HVSR of the broadband seismometer HV_ref (blue curve) and strong motion accelerometer HV_AC (orange curve) for IBRH10 and TKC respectively. In the case of IBRH10, we can see a clear peak at around 1 Hz for both sensors, but at 0.3 Hz, HV_AC is almost four time smaller than the HV_ref. This can be explained analyzing the Power Spectral Density (PSD) of the sensors, which showed that with the HV_AC we lose information in the low frequency range, where the components of the PSD are almost flat, this might be due to electric noise in the measuring instruments. The case of TKC is similar, we can see in Figure 1b that in the low frequency range, the HV_AC does not show any peak at 0.3 Hz. Without a broadband sensor we cannot obtain reliable information in the low frequency range. Figure 1c and Figure 1d show the dispersion curves of Rayleigh wave for the broadband sensors array DC_ref (blue curves) and short period sensors array (orange curves), in both cases we can see than the frequencies bellow 3 Hz cannot be covered with a short period array.

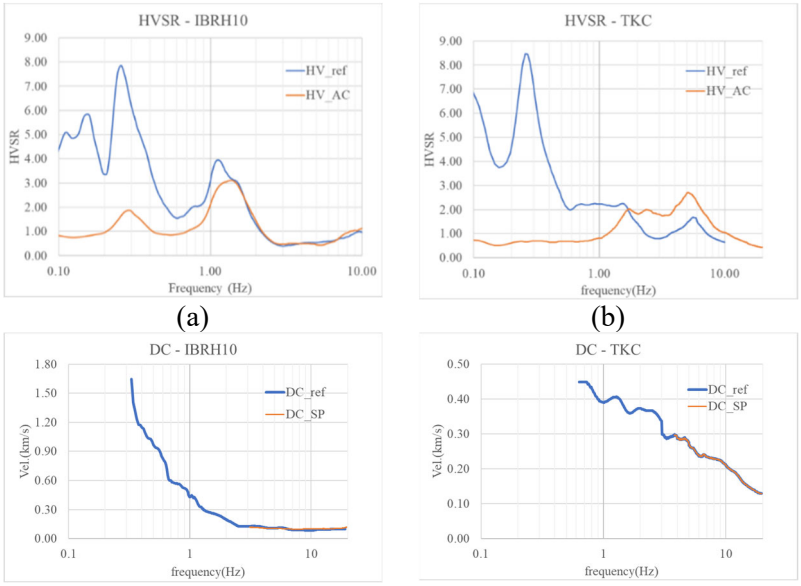

Figure 1. HVSR and dispersion curves of IBRH10 and TKC. (a) and (b) show HVSR of broadbad sensor (blue curves) and accelerometer (red curves). (c) and (d) show dispersion curve of the broadband sensor array (blue curves) and short period seismometers (orange curves)

The results of the joint inversion for IBRH10 is shown in Figure 2. The computed and observed models of HV and DC showed a good correlation in shape and amplitude, this gives as result the reference inverted P-wave and S-wave velocities, and density structure, which are shown in Figure 2a. We can observe a discontinuity at 570 m of depth, which indicates the presence of hard rock. This result of the inversion is acceptable by its similarity to the structure based on the PS-Logging.

Figure 2b shows the inverted velocity structure for the Case-1, using the HV_ref, and DC_SP. The observed curves and the computed ones show good correlation, and the results agree well with the reference model. Although the DC_SP cannot cover the frequency range below 3 Hz, the results indicate that this shortcoming is covered by the HV_ref. It can be pointed out that, even without a broadband array, we can obtain reliable results. For the Case-2 there was not a good correlation between the computed and observed models, therefore, we could not obtain any acceptable and reliable velocity structure.

The reference velocity - density structure for TKC, inverted from the HV_ref and DC_ref, is shown in Figure 3a. The computed HVSR and DC curves agree well with the observed HV_ref and DC_ref, showing a good correlation. In the velocity structure there is a clear discontinuity, a jump of Vs to a bigger than 1,000 m/sec, at around 510 m depth, which indicates the presence of hard rock. The structure below this clear discontinuity might be not reliable.

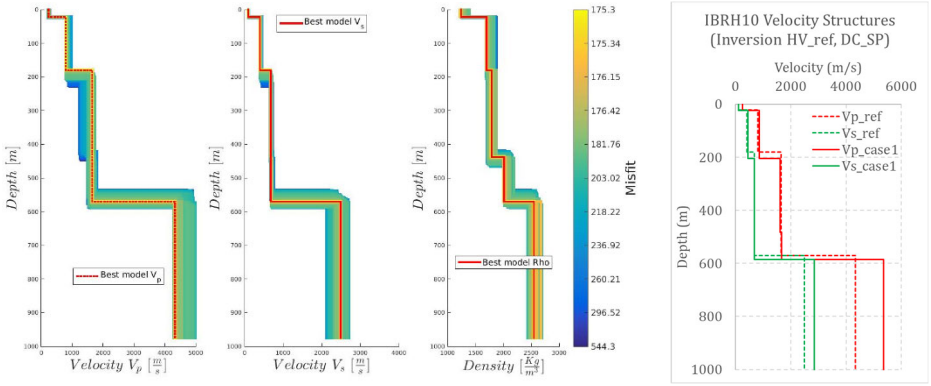

Figure 2. Results of the joint inversion for IBRH10. (a) shows the inverted velocities – density structure using HV_ref and DC_ref. Red lines indicate the best model among computed ones for Vp, Vs, and Density. The color scale indicates the misfit of the computed models with the observed data. (b) shows a comparison of the inverted velocity structures for IBRH10 between the velocity structure of Case-1 and the reference velocity structure. Broken lines indicate the reference velocity structure. Green lines indicate the S-wave velocity structure, whereas red ones the P-wave velocity structure.

In this site, any information obtained by drilling is not available. Neither shallow structure, nor deep one. We use this structure obtained from the HV_ref, and DC_ref as reference structure for TKC.

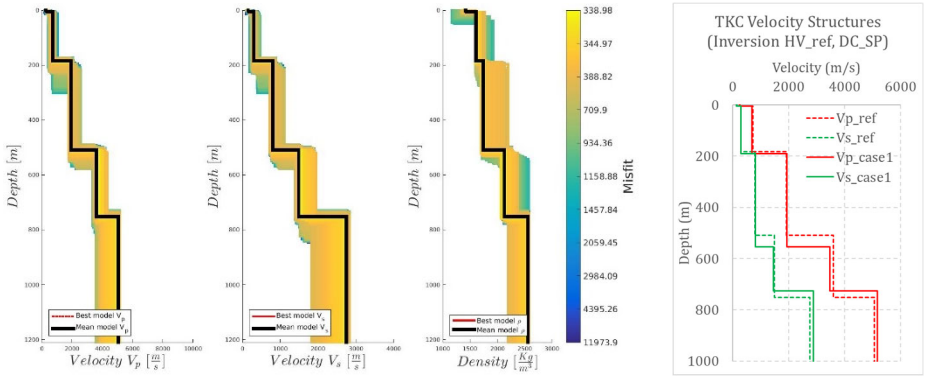

(a) (b)

Figure 3. Results of the joint inversion for TKC. (a) shows the inverted velocities – density structure using HV_ref and DC_ref. Black lines indicate the mean model for Vp, Vs, and Density among computed ones. (b) shows a comparison of the inverted velocity structures for TKC between the velocity structure of Case-1 and the reference velocity structure.

Figure 3b shows the inverted structure for the Case-1, using the HV_ref, and DC_SP for TKC. The observed curves and the computed ones using the inverted structure agree well, and the results are similar with the reference model. It can be pointed out that, even without a broadband array, we can obtain reliable results.

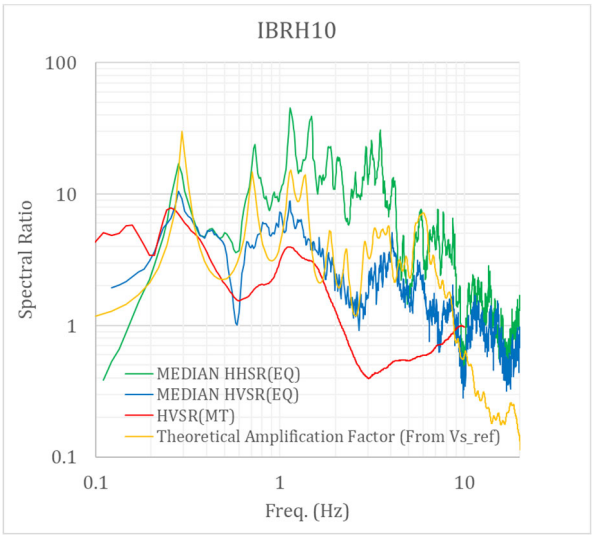

Figure 4. Comparison of the Theoretical Site Amplification Factor (from Vs_ref), HHSR(EQ), HVSR(EQ), and HVSR(MT).

Regarding Case-2, we could not obtain any reliable velocity structure. Using strong motion accelerometer for a single point measurement, and an array measurement composed of short period seismometers, it is very hard to obtain acceptable results because we do not have reliable information for the low frequency range.

Figure 4 shows the comparison of the theoretical amplification factor obtained from the reference velocity structure of IBRH10, with the HHSR(EQ), HVSR(EQ), and HVSR(MT). We can point out that the theoretical amplification factor is similar in shape to the HHSR(EQ), but it underestimates the amplitude of the peaks for frequencies larger than 0.7 Hz. All the spectral ratios show peaks at 0.3 Hz, and at around 1 Hz. Additionally, we can mention that HVSR(EQ) differs from HVSR(MT) on its amplitude, however, both show information of the bedrock in the low frequency range. Therefore, we cannot use the HVSR(EQ) as a proxy of HVSR(MT) to estimate the inverted velocity structure in case of the absence of a broadband sensor to perform single point microtremor measurement. Finally, we can see that above 1 Hz the amplitude of the HHSR(EQ) is the greatest, followed by the theoretical amplification factor, the HVSR(EQ), and the HVSR(MT) respectively. We can mention that the theoretical amplification factor, based on the estimated velocity structure using the joint inversion of the HV_ref and DC_ref, can give a good and reliable estimation of the amplification factor, but it still underestimates it. This might be due to the influence of the attenuation factor.

5. CONCLUSIONS

We determined the site characteristics with strong ground motion and microtremor records at two strong motion observation sites, IBRH10 and TKC. The data used in this study are strong motion records of 13

earthquakes for the KiK-NET station IBRH10, and microtremor single point measurements and array measurements in IBRH10 and TKC. For the strong motion records, we calculated the HVSR for the S-coda windows, and the HHSR for the S-wave windows using the bottom of the borehole as a reference site. We also calculated the HVSR for all the single point microtremor measurements, and divided them into two groups: HV_ref, which were calculated with the records obtained by a broadband seismometer; and HV_AC, with the records obtained by a strong motion accelerometer. Additionally, we estimated the dispersion curves of Rayleigh waves from the microtremor array measurements, we called DC_ref to the ones obtained with broadband seismometer array measurement, and DC_SP to the ones with short period seismometer array measurement. With the HVSR and DC, we performed the joint inversion for three different groups of analysis and obtained the S-wave velocity structure for each group. With this information, we calculated the theoretical site amplification factor for the IBRH10 station, and compared it to the HHSR, and HVSR of strong motion and microtremor records. The results are summarized as follows:

1. Using strong motion accelerometer to perform single point microtremor measurement we lose information in the low frequency range of the HVSR (HV_AC), where the peaks are very small or nonexistent due to its low sensitivity, while using a broadband sensor we obtain large peaks in the low frequency range.
2. For the dispersion curves of Rayleigh waves, we cannot cover the frequency range below 3 Hz using microtremor array measurements obtained by short period seismometers. Although the DC_SP cannot cover the frequency range below 3 Hz, the results of the joint inversion indicate that this shortcoming is covered by the HV_ref. Even without a broadband array, we can obtain a reliable velocity structure.
3. Without a broadband sensor, we cannot obtain a reliable velocity structure. For this analysis we need at least one broadband sensor of three components.
4. The theoretical amplification factor based on the estimated velocity structure using the joint inversion of the HV_ref and DC_ref, can give a good and reliable estimation of the amplification factor, but it still underestimates the amplification factor due to the influence of the attenuation factor.
5. The HVSR(MT) and HVSR(EQ) cannot be regarded as site amplification factor, but they allow us to obtain the frequency of the resonance peaks.
6. HVSR(EQ) cannot be considered as a proxy of HVSR(MT) for the joint inversion process, in case of the absence of a broadband sensor.

ACKNOWLEDGEMENTS

This research was conducted as the individual study of the training course “Seismology, Earthquake Engineering and Tsunami Disaster Mitigation” by IISEE/BRI, JICA, and GRIPS. I would like to express my sincere gratitude to my supervisor Dr. Toshiaki Yokoi, for his for this continuous support, guidance, and valuable comments during my individual study. I am also thankful with my co-supervisor Dr. Takumi Hayashida, for his suggestions and guidance.

REFERENCES

Aki, K., 1957. Bulletin of the Earthquake Research Institute, 35, 415-456.

Aki, K., 1965. Geophysics, 30(4), 493-667.

Arai, H., and Tokimatsu, K. (2004). Bulletin of the Seismological Society of America, 94(1), 53-63.

García-Jerez, A., Piña-Flores, J., Sánchez-Sesma, F. J., Luzón, F., & Perton, M. (2016). Computers & geosciences, 97, 67-78.

Okada, H., 2003. Geophysical Monograph Series Number 12.

Salinas, V., Luzón, F., García-Jerez, A., Sánchez-Sesma, F., Kawase, H., Matsushima, S., Campillo, M., 2014. Bulletin of the Seismological Society of America, 104(2), 995-1001.

Sánchez-Sesma, F. J., Rodríguez, M., Iturrarán-Viveros, U., Luzón, F., Campillo, M., Margerin, L., Rodríguez-Castellanos, A, 2011. Geophysical Journal International, 186(1), 221-225.